



Article

Safranin removal by fine soil: thermodynamics and kinetics of adsorption

Iraj Dehghanpour and Ghazaleh Kouchakzadeh 

Department of Chemistry, Khorramabad Branch, Islamic Azad University, Khorramabad, Iran

Abstract

Environmental problems caused by human intervention in nature are some of the most critical challenges facing human societies. It is essential to use suitable adsorbents to remove pollutants. The abundance, natural abundance and low cost of fine soil have made it a good candidate for removing environmental pollutants. In this research, removal of safranin dye by natural and acidic-organic-treated fine soil with sulfuric acid and ethanolamine was studied. The characteristics of natural and acidic-organic-treated fine soil were confirmed using X-ray diffraction, Fourier-transform infrared spectroscopy, Brunauer–Emmett–Teller and scanning electron microscopy techniques. The adsorbents were placed in contact with different concentrations of safranin dye solution separately. After that, the effects of adsorbent amount ($0.4\text{--}3.2\text{ g L}^{-1}$), contact time (0–60 min), adsorbate concentration (5–20 ppm) and pH (3–11) were evaluated regarding the optimum safranin adsorption process. The greatest adsorption capacity of fine soil was calculated as 1250 mg g^{-1} . The experimental results were evaluated using thermodynamic and kinetic models. The data showed that the process follows the Langmuir isotherm model and pseudo-second-order kinetic model. The intraparticle diffusion model estimated the possible mechanism of dye adsorption. Overall, it can be deduced that natural fine soil is an efficient remover of human pollutants.

Keywords: Adsorption, fine soil, Freundlich isotherm, Langmuir isotherm, safranin dye

(Received 16 February 2024; revised 17 May 2024)

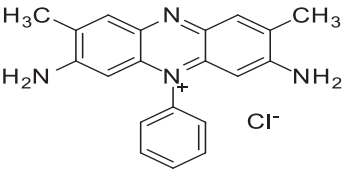
The application of green chemistry focuses on processes that reduce the production of hazardous substances. Moreover, minimizing production costs and using natural materials are significant considerations. Today, due to the presence of known contaminants and the emergence of new pollutants that are primarily the result of human activity, the environment and water supplies are increasingly becoming polluted. The use of green chemistry can be effective at preventing the development of environmental problems (Baloyi *et al.*, 2018; Cardona *et al.*, 2023). In recent years, various methods to remove pollutants from the environment and water supply using green chemistry approaches have been developed (Cardona *et al.*, 2023; Lezehari *et al.*, 2010). Several of these methods include biological treatment, membrane separation technology, advanced oxidation process, solvent extraction and adsorption (Ismail & Mokhtar, 2021; Casti *et al.*, 2022). Among these methods, adsorption can be a very efficient, economical and safe method for removing pollutants (Gupta *et al.*, 2011; Mahmoud *et al.*, 2020). Recently, much research has focused on the use of new and natural adsorbents (Bhatnagar *et al.*, 2010; Casti *et al.*, 2022). These novel adsorbents can include plant waste, fruit waste, bioadsorbents, waste materials left over from industry and agriculture and natural inorganic materials (Sharma *et al.*, 2011; Kyzas & Kostoglou, 2014; Ding *et al.*, 2015; Wahab *et al.*, 2019; Elaiyappillai *et al.*, 2021; Azizpourian *et al.*, 2023). Some researchers have focused their

attention on natural inorganic materials as adsorbents because natural materials are readily available and inexpensive. Fine soil is one such material. Particles of fine soil are not visible to the naked eye. Fine soil with a particle size $<2\text{ }\mu\text{m}$ is referred to as clay. The great interest in natural or modified clays is primarily attributed to their layered structure, large surface area, possibility of modification and easy accessibility (Bergaya & Lagaly, 2006; Lezehari *et al.*, 2010; Vicente *et al.*, 2013; Baloyi *et al.*, 2018; Guo *et al.*, 2018; Mahdi *et al.*, 2021). The negative charge of clays' layered structures are due to ionic substitutions in their crystal structures, increasing the ability of these minerals to adsorb cationic dyes (Shrivastava *et al.*, 1985; Gillott, 1987; Vicente *et al.*, 2013). Researchers have used clays as excellent adsorbents to adsorb dyes from the environment (İyim & Güçlü, 2009; Lezehari *et al.*, 2010; Shirsath *et al.*, 2011; Adebawale *et al.*, 2014; Fayazi *et al.*, 2015; Bentahar *et al.*, 2018; Kassimi *et al.*, 2021; Amrhar *et al.*, 2023; Silva *et al.*, 2023).

Safranin (3,7-diamino-2,8-dimethyl-5-phenyl phenazin-5-ium chloride) is a cationic dye and an azonium compound that is highly soluble in water (Chisholm, 1911; Kaur *et al.*, 2015; Sayed *et al.*, 2019). This dye is usually used for colouring cookies and sweets, as well as for dyeing wool, cotton, tannin, leather and paper (Kaur *et al.*, 2015; Sayed *et al.*, 2019; Suleman *et al.*, 2021). Safranin is used as a restaining agent in Gram staining and to detect the presence of glycosaminoglycans in meniscal structures (Shi *et al.*, 2021). However, the use of safranin in the food and drug industry is not safe, as this dye can have harmful effects on public health. The impacts of this dye on the skin, respiratory tract, cornea, lips and stomach have been proven (Fayazi *et al.*, 2015; Bensalah *et al.*, 2021). Because of this, environmentalists

Corresponding author: Ghazaleh Kouchakzadeh; Email: gh_kouchakzadeh@yahoo.com
Cite this article: Dehghanpour I, Kouchakzadeh G (2024). Safranin removal by fine soil: thermodynamics and kinetics of adsorption. *Clay Minerals* 59, 153–166. <https://doi.org/10.1180/clm.2024.15>

Table 1. Specifications of the safranin dye.

Compound	Chemical formula	Chemical structure	Molecular weight (g mol ⁻¹)	λ_{\max} (nm)
Safranin	C ₂₀ H ₁₉ ClN ₄		350.85	518

have advised that industrial wastewater containing safranin needs to be treated before it enters the environment (Azad *et al.*, 2015; Fayazi *et al.*, 2015). Much research has been carried out on the adsorption of safranin by different adsorbents (Lezehari *et al.*, 2010; Adebowale *et al.*, 2014; Fayazi *et al.*, 2015; Mohamed & Abukhadra, 2018; Derikvand *et al.*, 2019; Bensalah *et al.*, 2021; Shi *et al.*, 2021; Suleman *et al.*, 2021; Moradi *et al.*, 2022; Shwan, 2022; Uğraşkan *et al.*, 2022; Alkheraz *et al.*, 2023; Mohan *et al.*, 2023; Morrison *et al.*, 2023; Natal *et al.*, 2023; Shaltout *et al.*, 2024).

The present research deals with removing safranin dye from aqueous solution using natural and acidic-organic-treated fine soil. First, fine soil was prepared and then acidic-organic-treated fine soil synthesized. It is expected that acidic treatment affects the specific surface area of fine soil and removes some impurities from such samples (Boudriche *et al.*, 2011; Yarmohammadi *et al.*, 2022). Then, the effects of various parameters such as contact time, initial dye concentration, pH, temperature and adsorbent dosage on safranin removal by two adsorbents were investigated. The obtained findings were fitted to Langmuir, Freundlich and Temkin adsorption isotherms, and studies of adsorption kinetics were also carried out. The primary purpose of this work is to provide a method to remove safranin dye from aqueous solutions using available and suitable adsorbents. The importance of this method is related to the high efficiency of this natural adsorbent. To date, the removal of dyes has not been reported using the local fine soil employed in this work. As the fine soil used in this research has a diameter of <2 μm (Nooryazdan & Ghobadi, 2019), it is referred to as 'clay' here.

Materials and methods

Fine soil as a clay mineral was prepared using material from south-west Lorestan Province, Iran. Sodium chloride, sodium hydroxide, hydrochloric acid, sulfuric acid and ethanolamine were obtained from the Merck Company, all of analytical grade. Safranin (Sigma-Aldrich) was used as the adsorbate (Table 1). All solutions were prepared in distilled water.

Preparation of adsorbents

The clay mineral was washed with distilled water, sieved using a 200 μm meshed sieve and then dried at 95°C in an oven before use. The chemical composition of the used clay is given in Table 2, as assessed using X-ray diffraction (XRD).

This clay was used for the preparation of the acid-treated clay. The negative charge of the clay surface can be balanced with exchangeable cations such as Ca²⁺, Mg²⁺, Na⁺ and K⁺ (Braja & Dean, 2012). For this purpose, 10 g of initial clay was added to 500 mL of 1 M sodium chloride. The mixture was stirred

continuously for 3 h at room temperature and then washed with distilled water repeatedly. The resulting sample was dried at 60°C overnight. For acidic treatment, the resulting clay was placed in contact with 2 M sulfuric acid with a ratio of 1:50 for 2 h at 95°C (Kilislioglu & Aras, 2010; Viftaria *et al.*, 2019; Akbar *et al.*, 2022). In the following step, 10 g of acidic clay was dispersed in 600 mL of distilled water at room temperature using a stirrer for 24 h. Then, ethanolamine was added to the mixture at a ratio of 1:2, and it was stirred for 5 h at 80°C (Zawrah *et al.*, 2014). After 5 h, the sample was washed and dried at 90°C overnight, and then the acidic-organic-treated clay was stored for later use. The natural clay and acidic-organic-treated clay are named 'N-clay' and 'AO-clay', respectively, for ease of reference in the text.

Preparation of adsorbate

A stock solution of 100 mg L⁻¹ safranin dye was prepared by dissolving 100 mg in 1 L distilled water. Safranin dye is highly soluble in water, and the colour of the solution is red. Test solutions with concentrations of 5, 10, 15 and 20 ppm were prepared by diluting the stock solution. The maximum wavelength in the visible spectra region was determined as 518 nm using an ultraviolet-visible (UV-Vis) spectrophotometer (Perkin Elmer Lambda 25). The concentration calibration curve was drawn for the desired concentrations for later use.

Studies of dye removal

Batch experiments of dye removal were carried out in conical flasks with 25 mL of dye solution in contact with the adsorbents on a magnetic stirrer (VELP, Italy). The amount of residual dye in the desired solutions was determined using a UV-Vis spectrophotometer at regular time intervals after the samples were centrifuged (ALC, Italy). The experiments on the effects of concentration, contact time, pH and temperature were carried

Table 2. Chemical compositions of N-clay and AO-clay according to XRD results.

Compound	Composition	Formula
N-clay	Quartz	SiO ₂
	Calcite	CaCO ₃
	Dolomite	CaMg(CO ₃) ₂
	Albite	NaAlSi ₃ O ₈
	Clinocllore	(Na,Al) ₆ (Si,Al) ₄ O ₁₀ (OH) ₈
AO-clay	Muscovite	H ₂ KAl ₃ (SiO ₄) ₃
	Quartz	SiO ₂
	Gypsum	CaSO ₄ ·2H ₂ O
	Anhydrite	CaSO ₄
	Bassanite	CaSO ₄ ·0.5H ₂ O
	Albite, calcian	(Na,Ca)Al(Si,Al) ₃ O ₈

out to determine the optimum conditions for dye removal. The experiments were continued until dye concentration remained constant. When dye concentration achieved a constant value, the adsorption process had reached equilibrium. To determine the optimal amount of adsorbent, various doses of each adsorbent (0.4, 1.2, 2.0, 2.8 and 3.2 g L⁻¹) were placed in contact with the dye solution of the appropriate concentration. To evaluate the effects of initial concentration and contact time, the absorption of solutions with various concentrations (5–20 ppm) was first read using a UV–Vis spectrophotometer. A certain amount of adsorbent was added to the solutions, and the residual concentration was determined at regular time intervals. The pH effects were studied using 0.1 M HCl and 0.1 M NaOH to adjust the desired pH range from 3 to 11. To evaluate the influence of temperature, the experiments were conducted at 27°C, 37°C and 47°C. All experiments were repeated at least three times to ensure the accuracy of the obtained data. Following this, the amount of adsorbed dye at equilibrium condition (q_e) and the adsorption capacity of adsorbents at a time t (q_t) were estimated using Equations 1 & 2, respectively (Nourmoradi *et al.*, 2018; Żółtowska-Aksamitowska *et al.*, 2018; Pap *et al.*, 2020; Silva *et al.*, 2023):

$$q_e = \frac{(C_i - C_e)}{m} V \text{ (mg g}^{-1}\text{)} \quad (1)$$

$$q_t = \frac{(C_i - C_t)}{m} V \text{ (mg g}^{-1}\text{)} \quad (2)$$

where C_i , C_e and C_t are initial concentration, equilibrium concentration and concentration of safranin dye at time t (mg L⁻¹), respectively. In addition, m and V are the weight of the adsorbent (g) and dye solution volume (L), respectively. The removal percentage (R%) of safranin dye of the desired adsorbents was estimated using Equation 3 (Pouretedal & Sadegh, 2014; Banerjee *et al.*, 2016; Mondal *et al.*, 2016; Uygun *et al.*, 2023; Zeng *et al.*, 2023):

$$\text{R\%} = \frac{(C_i - C_e)}{C_i} \times 100 \quad (3)$$

Adsorption isotherms

Adsorption isotherms refer to the variation in the amount of adsorbate on the adsorbent surface with change in concentration at a constant temperature (Foo & Hameed, 2010). The adsorption isotherm can provide useful information regarding the adsorption process and adsorbent performance (Duan *et al.*, 2019; Uğraşkan *et al.*, 2022). Adsorption isotherm models include Langmuir, Freundlich and Temkin equations, which are widely used to describe the adsorption equilibrium process (Saha *et al.*, 2021; Azizpourian *et al.*, 2023). To study the adsorption isotherm in this work, experiments were performed using 2 g L⁻¹ of the desired adsorbent in 25 mL dye solution at pH 9 using various initial concentrations of safranin dye (5, 10, 15 and 20 ppm) for 40 min at three temperatures. When the adsorbate is bound with one functional group on the adsorbent surface, the Langmuir isotherm equation (Table 3) can describe the adsorption process (Langmuir, 1918; Baccar *et al.*, 2012; Banerjee *et al.*, 2016; Shaltout *et al.*, 2024). Freundlich's empirical equation shows the dependence between the amount of adsorbate on the

Table 3. Linear equations of the adsorption isotherm models.

Isotherm models	Linear equation	Parameters
Langmuir isotherm	$\frac{1}{q_e} = \left(\frac{1}{q_{\max}K_L}\right)\frac{1}{C_e} + \frac{1}{q_{\max}}$	q_e : the amount of drug adsorbed at equilibrium (mg g ⁻¹) q_{\max} : the maximum amount of drug adsorbed (mg g ⁻¹) K_L : adsorption equilibrium constant (L mg ⁻¹) C_e : the equilibrium concentration of drugs in solution (mg L ⁻¹)
Freundlich isotherm	$\ln(q_e) = \ln(K_F) + \left(\frac{1}{n}\right)\ln(C_e)$	K_F : adsorption capacity n : adsorption intensity
Temkin isotherm	$q_e = B\ln A + B\ln C_e$	B : coefficient of adsorption heat (J mol ⁻¹) A : coefficient of adsorption capacity (L mg ⁻¹)

adsorbent surface and the concentration of the solution (Banerjee *et al.*, 2016; Shaltout *et al.*, 2024). This isotherm is related to a heterogeneous surface (Mondal *et al.*, 2016; Saha *et al.*, 2021). For the Temkin isotherm, B and A are the coefficient of adsorption heat (J mol⁻¹) and coefficient adsorption capacity (L mg⁻¹), respectively (Chakravarty & Banerjee, 2012; Bassir & Shadizadeh, 2020). The linear equations of the Freundlich and Temkin isotherms are also given in Table 3. The Langmuir isotherm also describes the R_L parameter, which is a dimensionless number and indicates the nature of the adsorption. R_L was calculated using Equation 4:

$$R_L = \frac{1}{1 + K_L C_0} \quad (4)$$

where K_L is the adsorption equilibrium constant (L mg⁻¹) and C_0 is the initial concentration of the adsorbate (mg L⁻¹). When $0 < R_L < 1$, the Langmuir isotherm is favourable. However, if this parameter is equal to 1, the Langmuir isotherm is unfavourable (Mondal *et al.*, 2016; Alkherraz *et al.*, 2023; Shaltout *et al.*, 2024).

Table 4. Linear equations of the adsorption kinetic models.

Kinetic model	Linear equation	Parameters
Pseudo-first-order	$\ln(q_e - q_t) = \ln q_e - k_1 t$	q_e : equilibrium adsorption capacity q_t : adsorption capacity at time t k_1 : rate constant
Pseudo-second-order	$\frac{t}{q_t} = \frac{t}{q_e} + \frac{1}{k_2 q_e^2}$	q_e : equilibrium adsorption capacity q_t : adsorption capacity at time t k_2 : rate constant
Elovich	$q_t = \frac{1}{\beta} \ln(\alpha\beta) + \frac{1}{\beta} \ln(t)$	q_e : adsorption capacity at time t α : initial adsorption rate β : Elovich constant
Intra-particle diffusion	$q_t = k_{\text{dif}} t^{0.5} + C$	q_e : adsorption capacity at time t C : constant representing the thickness of the boundary layer k_{dif} : diffusion constant

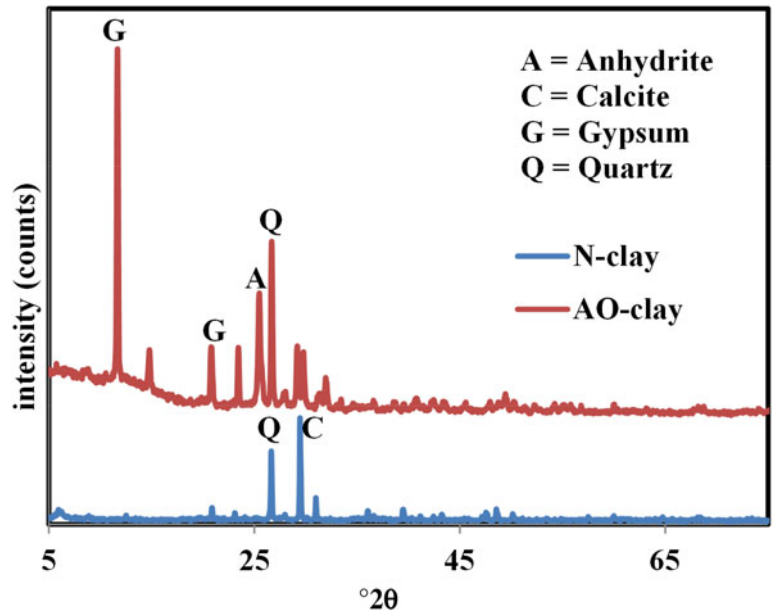


Figure 1. XRD traces of (a) N-clay and (b) AO-clay.

Adsorption thermodynamics and kinetics

Thermodynamic parameters play an important role when investigating adsorption behaviour (Banerjee *et al.*, 2016; Yurtay & Kılıç, 2023). The thermodynamic parameters, including ΔH° (enthalpy change; kJ mol^{-1}), ΔG° (Gibbs free energy change; kJ mol^{-1}) and ΔS° (entropy change; $\text{J mol}^{-1} \text{K}^{-1}$), can be evaluated using the Van 't Hoff equations (Equations 5–7):

$$K_0 = \frac{C_0 - C_e}{C_e}, \quad \Delta G^\circ = -RT \ln K_0 \quad (5)$$

$$\Delta G^\circ = \Delta H^\circ - T \Delta S^\circ \quad (6)$$

$$\ln(K_0) = \frac{\Delta S^\circ}{R} - \frac{\Delta H^\circ}{RT} \quad (7)$$

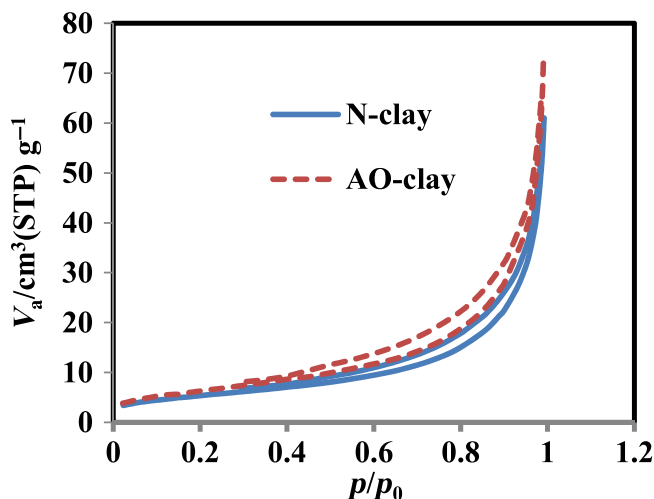


Figure 2. N_2 adsorption/desorption isotherms of N-clay and AO-clay. STP = standard temperature and pressure; V_a = total pore volume.

where K_0 is the equilibrium constant and T and R are temperature (K) and the universal gas constant, respectively (Chowdhury & Viraraghavan, 2009; Chakravarty & Banerjee, 2012; Morrison *et al.*, 2023; Njaramba *et al.*, 2023).

Linear kinetic equations can reasonably accurately determine the rate of safranin removal from a solution. Based on adsorption kinetics, the amount of adsorbate is measured with respect to time, and the experimental data are compared to kinetic models (Pouretedal & Sadegh, 2014; Bentahar *et al.*, 2018; Nourmoradi *et al.*, 2018; Yin *et al.*, 2018; Lima *et al.*, 2021; Abbou *et al.*, 2022).

In this work, pseudo-first-order, pseudo-second-order, Elovich and intraparticle diffusion models (Guo *et al.*, 2015; Largitte & Pasquier, 2016; Manjuladevi *et al.*, 2018; Edet & Ifelebuegu, 2020; Wang *et al.*, 2021; Hongswat & Prarat, 2022; Uğraşkan *et al.*, 2022) were used to determine the type of adsorption kinetics observed (Table 4). Two significant aspects of the intraparticle diffusion model are the film diffusion (D_F) and intraparticle diffusion (D_P) coefficients. The D_F coefficient determines whether an adsorption process is controlled by film diffusion and the D_P coefficient reflects control of the adsorption process by intraparticle diffusion (Equations 8 & 9):

$$D_F = \frac{0.23r_0\Gamma C_S}{C_L t_{0.5}} \quad (8)$$

$$D_P = \frac{0.03r_0^2}{t_{0.5}} \quad (9)$$

where r_0 (cm) and Γ are the radius of the adsorbent particle and film thickness, respectively, $t_{0.5}$ is the time necessary to complete half of the process (min) and C_S and C_L are the substrate concentrations in the solid and solution at t time, respectively. When D_P is the range 10^{-11} – $10^{-13} \text{ cm}^2 \text{ s}^{-1}$, it can be stated that the process rate is controlled by the intraparticle diffusion. When D_F is in the range of 10^{-6} – $10^{-8} \text{ cm}^2 \text{ s}^{-1}$, the rate of adsorption process is controlled by film diffusion (Sepehr *et al.*, 2014; Obradović, 2020).

The study of adsorption thermodynamics and kinetics was carried out at three temperatures (27°C, 37°C and 47°C) under

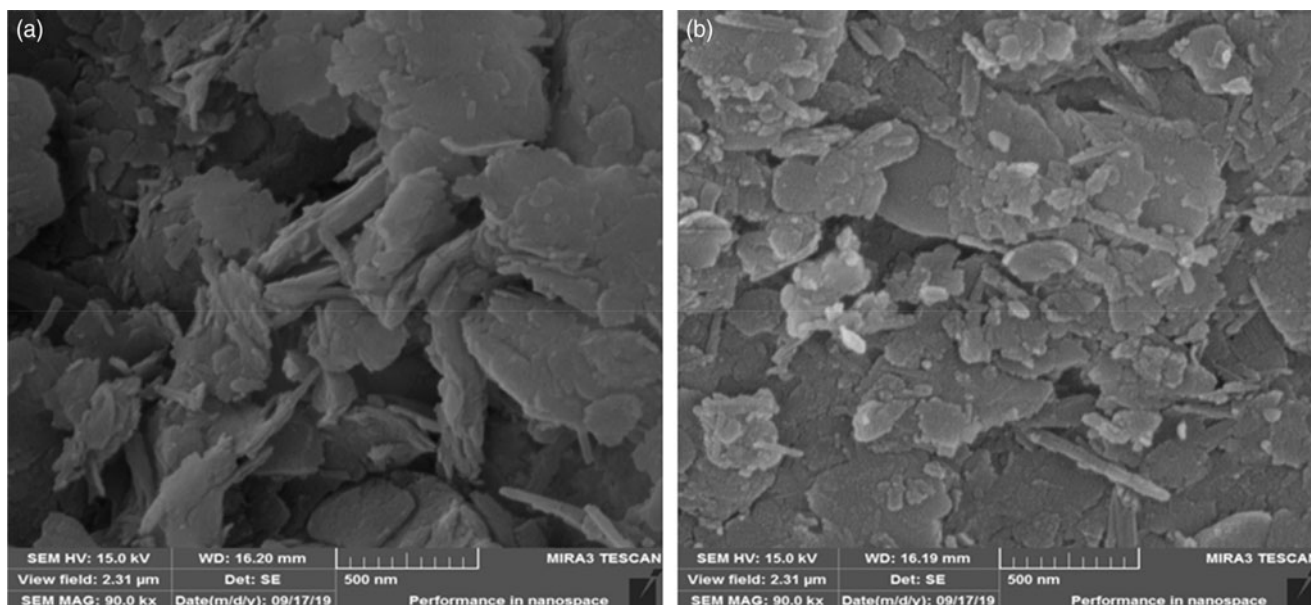


Figure 3. SEM images of (a) N-clay and (b) AO-clay.

optimal conditions of concentration, pH and amount of adsorbent.

Results and discussion

Characterization of adsorbents

N-clay and AO-clay were identified using an XRD instrument (Bruker, Germany), and their traces are displayed in Fig. 1. These traces were taken using a Cu-K α source ($\lambda = 0.154$ nm). As mentioned in Table 2, fine soils contain various clay minerals. The clearest peaks for N-clay and AO-clay were calcite and gypsum, respectively, and other minerals were found in minor quantities. Clay modification caused changes the structure of the AO-clay (Fig. 1b). Calcite and dolomite minerals were altered, and gypsum, anhydrite and basanite minerals were produced. In addition, by comparing Fig. 1a and Fig. 1b, it can be estimated that, due to the decrease in the intensity of the quartz, montmorillonite and calcite peaks, the cohesion of the layers decreased.

The values of the peaks at the diffraction angle $2\theta \approx 32$ correspond to the quartz phase (Ding *et al.*, 2015), and the intensity of the quartz peak is different in the desired adsorbents. According to these data, the basal spacing of AO-clay was more significant than the basal spacing of N-clay. The basal spacings of N-clay and AO-clay were estimated using Bragg's law (Haoue *et al.*, 2020) at ~ 2.95 and 7.32 Å, respectively. The increase in the basal spacing of AO-clay may be attributed to the intercalation of ethanolamine in the interlaminar space of the clay (Christidis, 2012; López-Chavez *et al.*, 2017; Shivaraju *et al.*, 2018).

The specific surface area and pore volume of the desired adsorbents were determined using the Brunauer–Emmett–Teller (BET) method (Fig. 2). Figure 2 shows that the hysteresis loop is similar to type H3. These particles are flexible and expandable and contain slit-shaped pores (Panda *et al.*, 2010). The BET-specific surface areas were estimated at 25.180 and 23.472 m² g⁻¹ for N-clay and AO-clay, respectively. The pore volume values were also reported to be 5.78 and 4.69 m³ g⁻¹ for N-clay and AO-clay, respectively. According to the BET results, the desired adsorbents

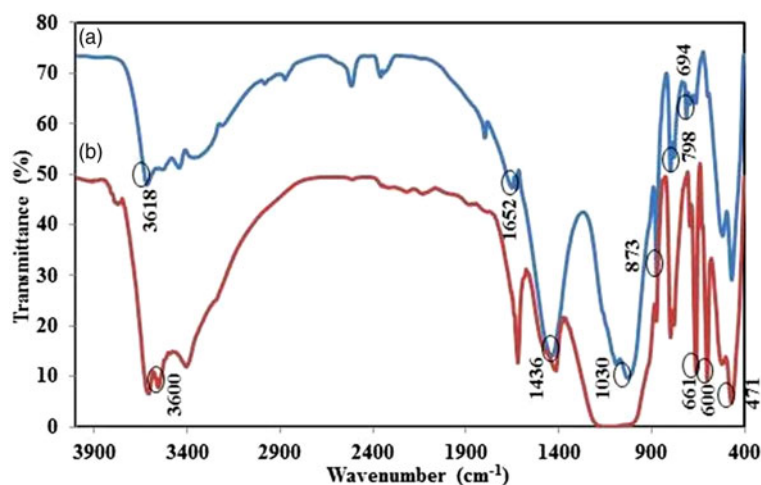


Figure 4. FTIR spectra of (a) N-clay and (b) AO-clay.

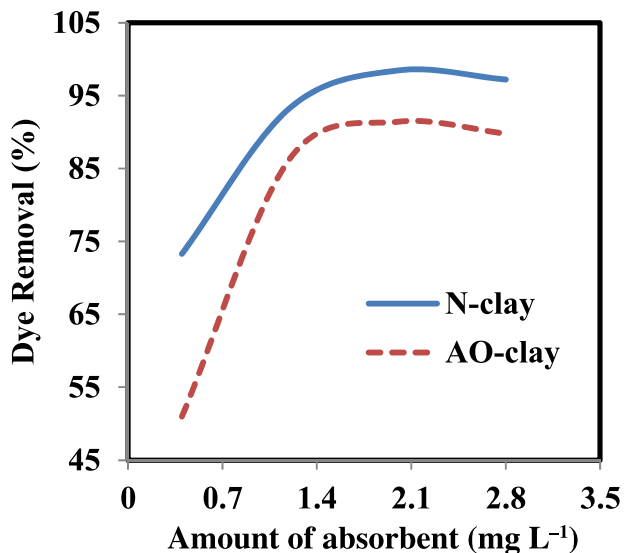


Figure 5. Effect of adsorbent dose on the performance of N-clay and AO-clay adsorbents (dye concentration = 20 ppm, contact time = 40 min, aqueous medium, temperature = 25°C).

were identified as mesoporous materials with mean pore diameters of 9.28 and 17.33 nm for N-clay and AO-clay, respectively. These results show that the clay layers were slightly separated and that they underwent good cleavage in one or two directions, creating thin plates (Ruiz-Agudo *et al.*, 2016). In addition, the specific surface area after the adsorption process of the natural clay adsorbent was found to be 20.413 m² g⁻¹.

Scanning electron microscopy (SEM) imaging was used to characterize the morphology of the desired adsorbents (Fig. 3) using a MIRA3 TESCAN SEM device (Czechia). The difference in the morphology of the desired adsorbents is due to the change in the structure of the AO-clay adsorbent. Figure 3a shows the N-clay structure taking the form of sheets and glossy layers containing calcite, quartz and montmorillonite minerals (Perri *et al.*,

2008; Chen *et al.*, 2011; Christidis, 2012; Choi *et al.*, 2017; Guo *et al.*, 2018). As can be seen in Fig. 3b, rod structures can be attributed to the gypsum and anhydrite minerals in AO-clay.

Fourier-transform infrared (FTIR) spectroscopy was used to characterize molecular bonding in the adsorbents (Fig. 4) using a Perkin-Elmer Spectrum RXI FTIR spectrophotometer (USA) with a KBr pellet in the range of 4000–400 cm⁻¹. Most bands in Fig. 4 were found between 450 and 1100 cm⁻¹. The peaks in the range of 670–797 cm⁻¹ may be attributed to the Si–O and Si–O–Al stretching vibrations of the quartz mineral in the desired adsorbents (Rezende *et al.*, 2018; Marsh *et al.*, 2019; Shwan, 2022). In AO-clay, a weak doublet peak in the range of 602–662 cm⁻¹ may be related to the in-plane and out-of-plane bending vibrations of SO₄²⁻ (Kamaraj *et al.*, 2017). In N-clay, the absorption peak at ~1652 cm⁻¹ can be attributed to the presence of adsorbed water in the material (Rezende *et al.*, 2018). Additionally, the bands at ~3400 and ~3700 cm⁻¹ correspond to OH group vibration elongations (Boudriche *et al.*, 2011; Rezende *et al.*, 2018; Azizpourian *et al.*, 2023).

Investigating the adsorption of safranin dye

Effect of adsorbent dose

The effect of the adsorbent dose on the adsorption of safranin was first evaluated using various amount of the desired adsorbent. The preliminary experiments showed that the desired adsorbent can remove the dye in a very short time, so the highest concentration of safranin was chosen to determine the effect of the amount of adsorbent. The best adsorbent amount in 20 ppm safranin solution was reported as 2 g L⁻¹ for N-clay and AO-clay. The highest percentages of dye removal for the optimal amount of adsorbent were 98.4% and 91.4% for N-clay and AO-clay, respectively (Fig. 5). A decrease in removal efficiency after achieving adsorption equilibrium may indicate that the dye molecules accumulated at the adsorbent sites (Pouretedal & Sadegh, 2014; Derikvand *et al.*, 2019). These optimal amounts of adsorbent were used in the subsequent experiments.

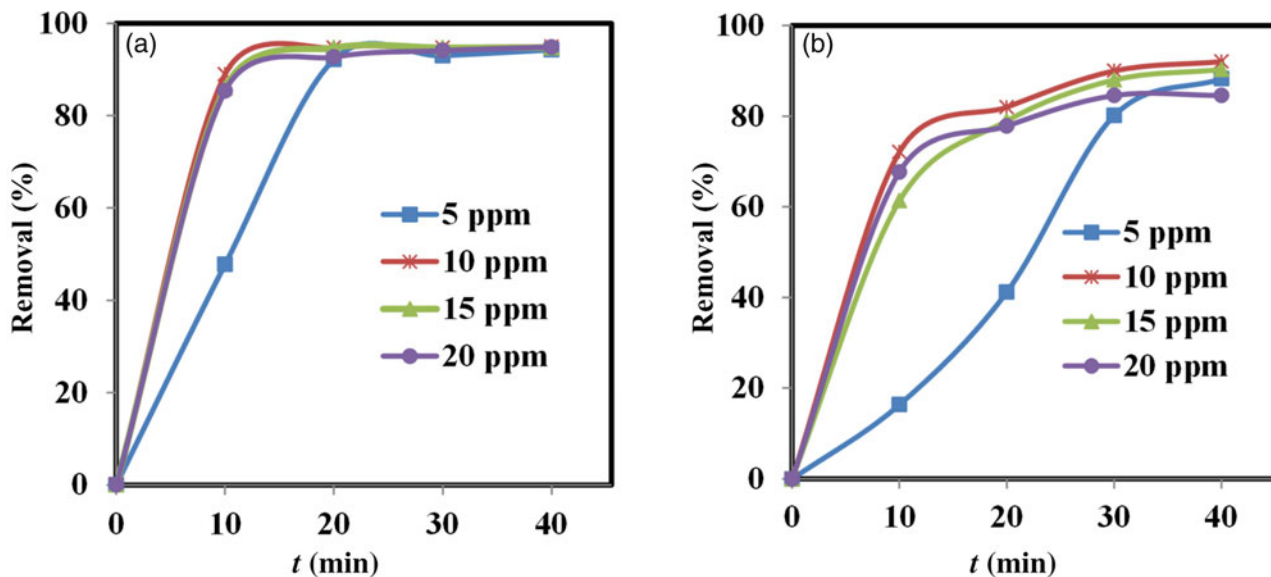


Figure 6. Effects of contact time and concentration on the performance of (a) N-clay and (b) AO-clay adsorbents (adsorbent dose = 2 g L⁻¹, aqueous medium, temperature = 25°C).

Table 5. Comparative results regarding the effects of initial dye concentration and contact time for different adsorbents.

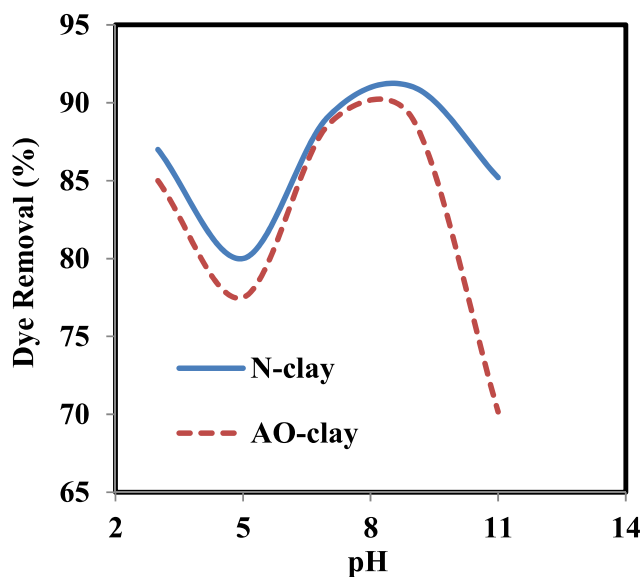
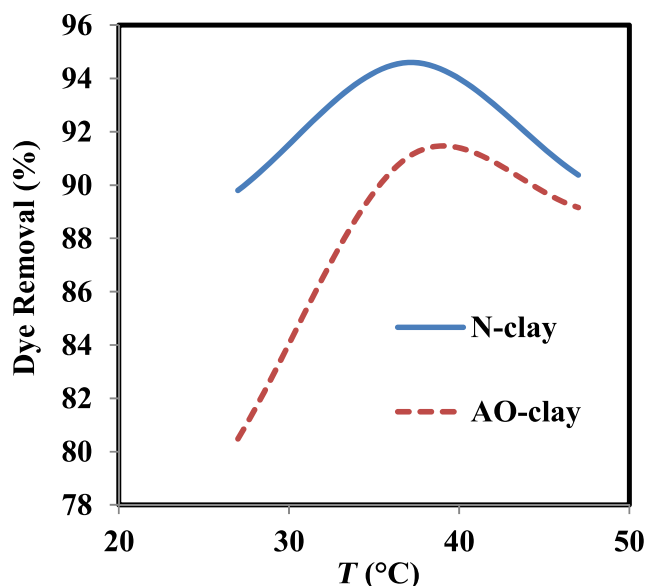
Adsorbent	Removal (%)	Concentration (ppm)	Contact time (min)	Adsorbent dose (g L ⁻¹)
N-clay	93.12 ^a	10.0 ^a	20 ^a	2 ^a
AO-clay	92.03 ^a	10.0 ^a	40 ^a	2 ^a
Kaolinite clay	90.00 ^b	100.0 ^b	40 ^b	5 ^b
Natural clay	100.00 ^c	50.0 ^c	180 ^c	5 ^c
Pillared clay	90.00 ^d	135.0 ^d	180 ^d	60 ^d
Magnetic clay	88.47 ^e	60.0 ^e	20 ^e	1 ^e

^aThis work.^bAdebowale *et al.* (2014).^cShwan (2022).^dLezehari *et al.* (2010).^eFayazi *et al.* (2015).

Effects of initial concentration and contact time

The adsorption process depends on the initial adsorbate concentration and the contact time (Banerjee *et al.*, 2016). At the optimal contact time, the adsorption process can reach equilibrium. Figure 6 & Table 5 show the effects of initial dye concentration and contact time on dye removal by N-clay and AO-clay adsorbents.

The value of dye removal percentage in contact with 2 g L⁻¹ adsorbent was calculated using Equation 3. The greatest dye removal percentages were found to be 93.12% in contact with N-clay after 20 min and 92.03% in contact with AO-clay after 40 min. The adsorption process was nearly constant after 20 and 40 min for N-clay and AO-clay, respectively (Fig. 6), and the process reached equilibrium. We can predict that the dye molecules would be located on the surface of the N-clay, whereas they would be located along the cleavages of the AO-clay. This difference in the function of adsorbents leads to decreasing the time to establish equilibrium in adsorption for the N-clay adsorbent. The efficiency of the adsorbent reduced with increasing concentration, and this may be due to the occupation of the active sites of the adsorbent by the adsorbate (Banerjee *et al.*, 2016).

**Figure 7.** Effect of pH on the performance of N-clay and AO-clay adsorbents (dye concentration = 10 ppm, adsorbent dose = 2 g L⁻¹, contact time = 40 min, pH = 3–11, temperature = 25°C).**Figure 8.** Effect of temperature on the performance of N-clay and AO-clay adsorbents (dye concentration = 10 ppm, adsorbent dose = 2 g L⁻¹, contact time = 40 min, pH = 9).

Effect of pH

pH is a significant parameter that can affect the adsorption capacity and properties of adsorbates and adsorbents (Tezcanli-Güyer & Ince, 2004; Mohamed & Abukhadra, 2018; Bernal *et al.*, 2020). To determine the optimal pH in the process of safranin removal, various pH values ranging from 3 to 11 were investigated. With increasing pH from 3 to 11, the dye removal percentage varied such that the maximum dye removal percentages were 88.93% at pH 9 for the AO-clay adsorbent and 91.9% at pH 9 for the N-clay adsorbent (Fig. 7).

The clay's layered structure has a mostly negative charge; therefore, it can interact with dye molecules that possess a positive charge (Shrivastava *et al.*, 1985). The surface charge of the adsorbent, the functional groups, the adsorbate charge and the

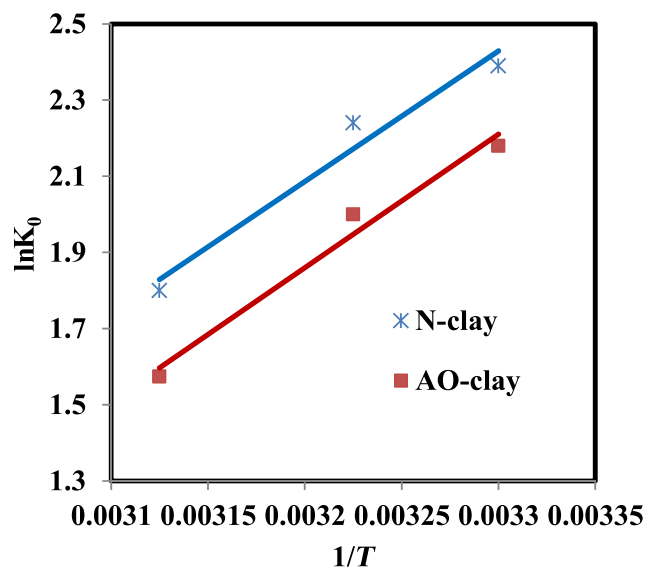
**Figure 9.** Plot of $\ln K_0$ vs $1/T$ (dye concentration = 10 ppm, adsorbent dose = 2 g L⁻¹, contact time = 40 min, pH = 9).

Table 6. Thermodynamic parameters for the removal of safranin dye by N-clay and AO-clay adsorbents (dye concentration = 10 ppm, adsorbent dose = 2 g L⁻¹, contact time = 40 min, pH = 9).

Adsorbent	T (°C)	K ₀	G° (kJ mol ⁻¹)Δ	ΔH° (kJ mol ⁻¹)	ΔS° (J mol ⁻¹)
N-clay	27	10.94	-6.34	-28.5	-73.8
	37	9.39	-5.60		
	47	6.05	-4.80		
AO-clay	27	8.86	-5.44	-29.2	-77.8
	37	8.16	-5.41		
	47	4.82	-4.19		

pH of the solution can affect the dye removal percentage. At pH 3, we may assume that as the surface charge of the adsorbent is more negative than at pH 5, the interaction between adsorbent and adsorbate increases and the dye removal percentage improves. At basic pH, the dye removal percentage and electrostatic interactions increase due to the presence of hydroxyl ions.

Table 7. Comparison of safranin adsorption capacity as determined by this work with results from other researchers.

Adsorbent	Maximum adsorption capacity	Reference
N-clay	1250 mg g ⁻¹	This work
AO-clay	625 mg g ⁻¹	This work
Pillared clay	536 μmol g ⁻¹	Lezehari <i>et al.</i> (2010)
Kaolinite clay	16.23 mg g ⁻¹	Adebowale <i>et al.</i> (2014)
Magnetic clay	18.48 mg g ⁻¹	Fayazi <i>et al.</i> (2015)
Sepiolite clay	20 mmol kg ⁻¹	Sieren <i>et al.</i> (2020)
Kaolinite clay	34 mmol kg ⁻¹	Hebert <i>et al.</i> (2020)
Natural clay	82.4 mg g ⁻¹	Shwan (2022)
Clay-based membrane	108 mg g ⁻¹	Mohan <i>et al.</i> (2023)

At higher pH values, the dye removal percentage decreases due to occupation of the active sites of the adsorbent (El-Kemary *et al.*, 2011; Kassimi *et al.*, 2021; Suleman *et al.*, 2021; Mohan *et al.*, 2023).

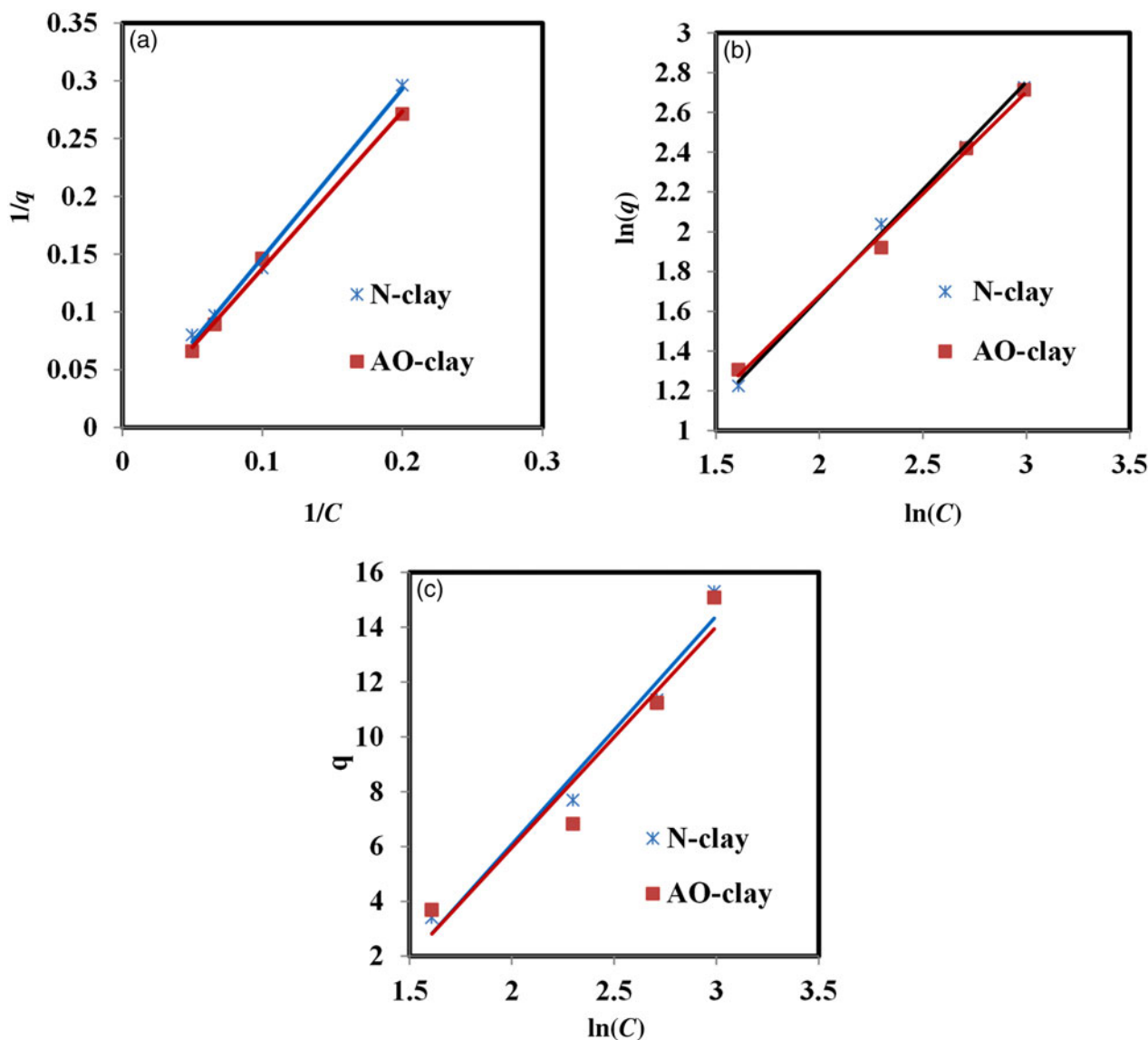


Figure 10. Plots of the (a) Langmuir, (b) Freundlich and (c) Temkin adsorption isotherms (dye concentration = 10 ppm, adsorbent dose = 2 g L⁻¹, contact time = 40 min, pH = 9, temperature = 37°C).

Table 8. Evaluated parameters for the safranin dye adsorption isotherms (dye concentration = 10 ppm, contact time = 40 min, pH = 9).

Adsorbent	Langmuir			R_L	Freundlich			Temkin		
	K_L (L mg ⁻¹)	q_m (mg g ⁻¹)	R^2		n	K_F (L g ⁻¹)	R^2	A (L g ⁻¹)	B (J mol ⁻¹)	R^2
N-clay	5.47×10^{-4}	1250	0.996	0.98	0.924	0.609	0.998	0.277	8.215	0.968
AO-clay	1.17×10^{-3}	625	0.996	0.98	0.976	0.689	0.995	0.284	8.046	0.937

Effect of temperature and determination of thermodynamic parameters

Temperature can have a significant impact on the dye removal percentage and thermodynamics of adsorption (Banerjee *et al.*, 2016; Bentahar *et al.*, 2018). In this study, the effect of temperature was examined at various temperatures: 27°C, 37°C and 47°C. The obtained results show that the dye removal percentage increases from 27°C to 37°C and decreases from 37°C to 47°C. The optimal temperature in the dye removal process occurred at 37°C, and the dye removal percentages were 94.6% and 91.1% when in contact with N-clay and AO-clay adsorbents, respectively.

According to Fig. 8, the decrease in the dye removal percentage at 47°C might be due to the increase in the movement of dye molecules to different adsorbent sites (Albroomi *et al.*, 2016) or to the weak bonds between the dye and the adsorbent surface (Banerjee *et al.*, 2016). Studying the effect of temperature on the safranin removal process can help us to evaluate thermodynamic parameters such as ΔH° , ΔG° and ΔS° using Equations 5–7. ΔH° and ΔS° can be calculated by plotting $\ln K_0$ vs $1/T$, so that, based on Equation 7, these parameters can be estimated from the values of the slope and the intercept (Xu *et al.*, 2012).

The results show that the ΔG° values are negative and the adsorption process can be spontaneous (Fig. 9 & Table 6). The ΔH° and ΔS° values are also negative. The negative value of ΔH° indicates that the adsorption process is exothermic, and the value of ΔS° indicates decreased randomness at the solid–liquid interface during the adsorption process (Xu *et al.*, 2012). When the AO-clay adsorbent was placed in solution, its anhydrite molecules can hydrolyse; therefore, the process is

more exothermic than the process of adsorption when in contact with N-clay.

By determining the optimum conditions of safranin adsorption using N-clay and AO-clay adsorbents in this work, we can compare these results with recent work conducted by other researchers (Table 7). In this research, the optimum conditions are dye concentration = 10 ppm, adsorbent dose = 2 g L⁻¹, contact time = 40 min and pH = 9.

Study of adsorption isotherms

Adsorption isotherms were investigated using the equations shown in Table 3. Figure 10 indicates the plots of Langmuir, Freundlich and Temkin isotherms for the adsorption of safranin dye on the desired adsorbents. Table 8 summarises the Langmuir, Freundlich and Temkin parameters obtained from the slopes and the intercepts of the plots.

Comparing the values of the correlation coefficients indicated an excellent fit for both the Langmuir and Freundlich isotherms, whereas the experimental data for the Temkin isotherm fitted less accurately. According to the obtained results, the data fitted the Langmuir model best.

The Langmuir isotherm model indicates that the active sites on the surface are equivalent. By contrast, the Freundlich isotherm model indicates that the difference in the nature of the surface of the materials depends on interactions between the functional groups of the adsorbate and the adsorbent molecules (Irandoost *et al.*, 2019).

Adsorption kinetics

The adsorption speed is the main factor impacting the adsorption process. The properties of the adsorbent and the adsorbate affect the adsorption mechanism (Irandoost *et al.*, 2019; Azizpourian *et al.*, 2023). The type of adsorption kinetics and kinetic parameters were estimated using pseudo-first-order, pseudo-second-order, Elovich and intraparticle diffusion models for the removal of safranin at various contact times by the desired adsorbents. The correlation coefficients of these kinetic models indicated that the pseudo-second-order model fits the dye adsorption results better than the pseudo-first-order model, and the $q_{e,cal}$ values were nearly in accordance with the $q_{e,exp}$ values (Table 9).

Comparing the R^2 values of the pseudo-second-order model for the desired adsorbents indicates that safranin was removed by the N-clay adsorbent better than by the AO-clay adsorbent (Table 9). Figure 11 displays the plots of these kinetic models.

The intraparticle diffusion model proposed by Weber and Morris (Kassimi *et al.*, 2021; Amrhar *et al.*, 2023) was used to study the migration of the safranin solution to the adsorbent surface. The values of k_{dif} and C were calculated from the slopes and the intercepts of the plots of q_t vs $t_{1/2}$, respectively (Roosta *et al.*, 2015; Sharma *et al.*, 2024).

Table 9. Evaluated parameters for safranin adsorption with various kinetic models (dye concentration = 10 ppm, adsorbent dose = 2 g L⁻¹, contact time = 40 min, pH = 9, temperature = 37°C).

Kinetic model	Parameters	N-clay	AO-clay
Pseudo-first-order	k_1 (min ⁻¹)	0.051	0.120
	R^2	0.814	0.963
	$q_{e,1}^*$ (mg g ⁻¹)	8.500	9.080
	$q_{e,exp}^*$ (mg g ⁻¹)	7.700	10.900
Pseudo-second-order	k_2 (M ⁻¹ min ⁻¹)	0.146	0.0362
	R^2	0.999	0.999
	$q_{e,2}^*$ (mg g ⁻¹)	7.924	11.100
	$q_{e,exp}^*$ (mg g ⁻¹)	7.700	10.900
Elovich	β	0.861	0.614
	α	19 844.1	258.72
	R^2	0.935	0.982
	k_{dif1}	0.499	0.520
Intraparticle diffusion	C_1	12.490	10.010
	R^2	0.883	0.907
	k_{dif2} (mg g ⁻¹ min ^{-0.5})	0.039	0.023
	C_2 (mg g ⁻¹)	15.530	12.990
	R^2	0.906	0.972
	D_f (cm ² s ⁻¹)	3.19×10^{-6}	2.92×10^{-7}
	D_p (cm ² s ⁻¹)	3.75×10^{-17}	1.79×10^{-15}

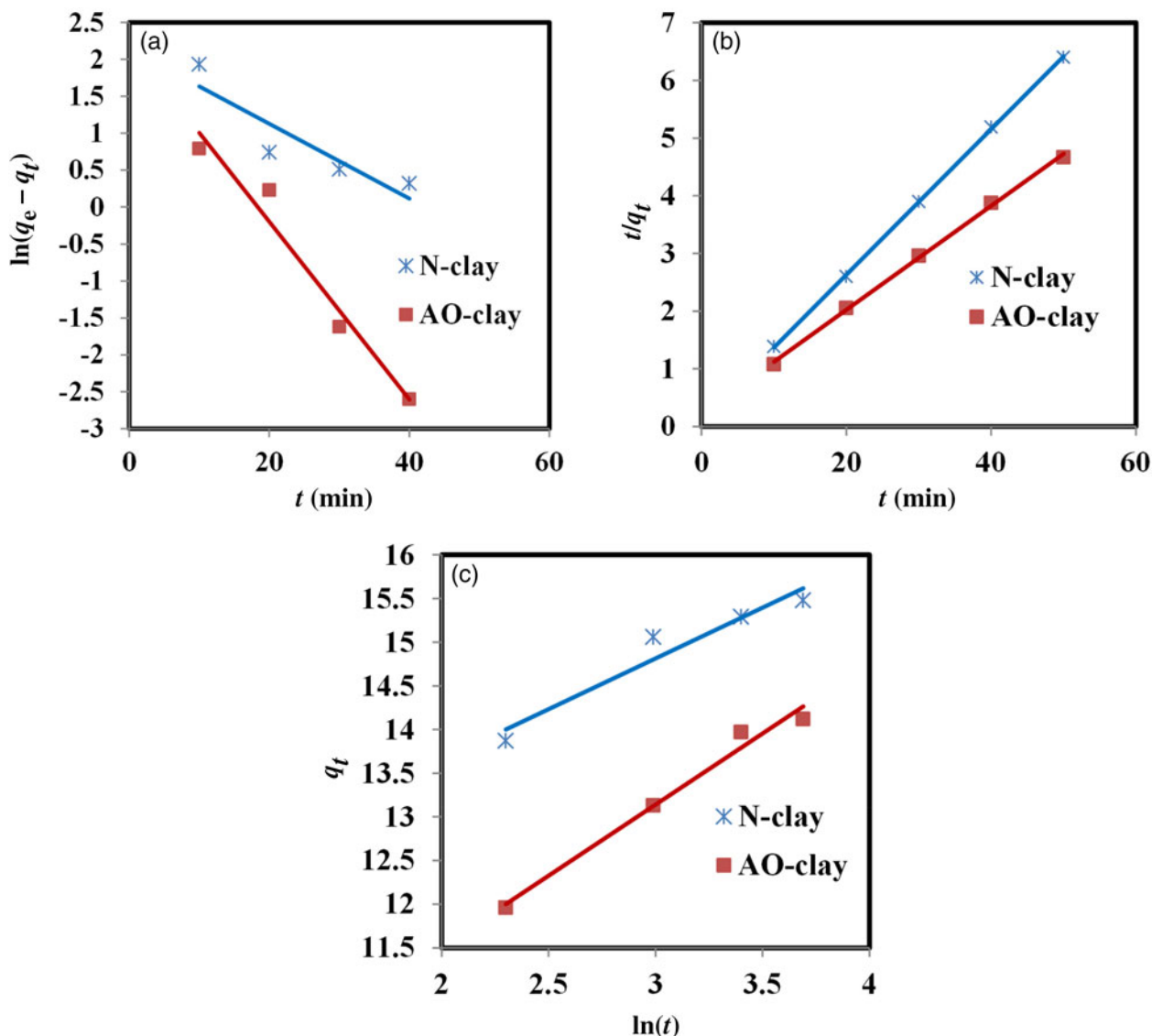


Figure 11. Plots of the (a) pseudo-first-order, (b) pseudo-second-order and (c) Elovich kinetic models (dye concentration = 10 ppm, adsorbent dose = 2 g L⁻¹, contact time = 40 min, pH = 9, temperature = 37°C).

As Fig. 12 shows, these plots did not pass through the origin, so the adsorption process consists of two steps. The first one is the migration of the adsorbate solution to the adsorbent surface, and the second one is the intraparticle diffusion of the substance into the adsorbent pores (Haleta *et al.*, 2009; Sepehr *et al.*, 2014; Campos *et al.*, 2018; Kuang *et al.*, 2020).

The first step has a sharp slope, and then it slows until reaching the equilibrium state (Fig. 12). It seems that dye molecules first transfer from the solution to the adsorbent surface, and the adsorption capacity increases from the initial time until 40 min.

The intercept value of C displays a lag time (Sepehr *et al.*, 2014; Obradović, 2020) of $t_{lag} = 0.9$ min for the mass transfer of the solution to the adsorbent surface, reflecting a delay of ~ 0.81 min in the adsorption process. However, the positive and high values of the intercept (C) indicate that the influence of the boundary layer is significant, and this is in agreement with the results regarding intraparticle diffusion (D_p) and film diffusion (D_f). The values of D_p and D_f were calculated as 1.79×10^{-15} and 2.92×10^{-7} cm²/s, respectively, for the AO-clay

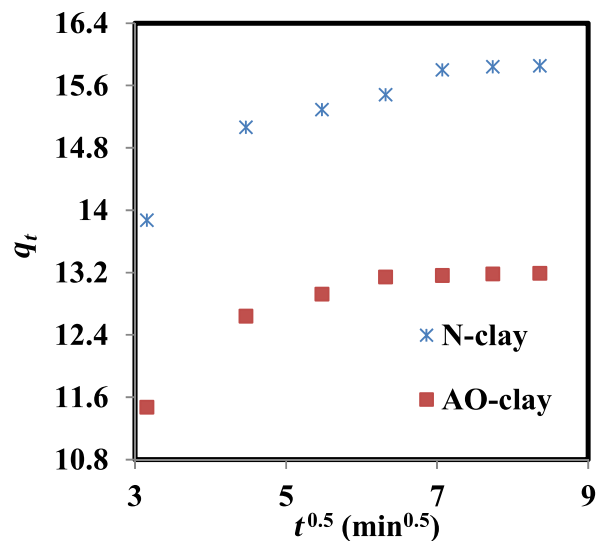


Figure 12. Plot of the intraparticle diffusion model (dye concentration = 10 ppm, adsorbent dose = 2 g L⁻¹, contact time = 40 min, pH = 9, temperature = 37°C).

adsorbent and as 3.75×10^{-17} and 3.19×10^{-6} , respectively, for the N-clay adsorbent. These results indicate that the rate-limiting step is film diffusion and that internal transmission dominates over external transmission (Karthikeyan *et al.*, 2010).

Conclusion

This research demonstrates the importance of using an inexpensive and locally obtained adsorbent to remove safranin dye from aqueous solutions. The adsorption process of the dye was carried out by fine soils called N-clay and AO-clay. The experimental results showed that the ability of N-clay to adsorb dye is slightly higher than that of AO-clay. It can be seen that when natural clays change, they do not necessarily become better adsorbents. The XRD results showed that the main difference between N-clay and AO-clay relates to the presence of calcite and gypsum. The results of the various experiments on the removal of safranin showed that optimum conditions occurred at a dye concentration of 10 ppm with pH 9, with an adsorbent dose of 2 g L^{-1} and at 37°C . At these optimum conditions, N-clay and AO-clay adsorbed 94.6% and 91.1% of safranin dye after 40 min, respectively. Despite the greater specific surface area of AO-clay compared to N-clay, the adsorption efficiency of N-clay was greater than that of AO-clay. Safranin dye can be rapidly adsorbed on the surface of N-clay, whereas the process of adsorption can occur along the cleavages of AO-clay. This adsorption evaluation indicated that the adsorption data fit the Langmuir and Freundlich models and the kinetic data fit the pseudo-second-order model. The maximum adsorption capacities of dye removal by N-clay and AO-clay were 1250 and 625 mg g^{-1} , respectively. Thermodynamic analysis of the dye removal demonstrated that this process is exothermic and spontaneous, with decreasing entropy. The evaluation of the intraparticle diffusion model revealed that the adsorption rate increases until ~ 40 min and then slowed down. According to the results of this model, the rate-limiting step was film diffusion, confirming the applicability of the pseudo-second-order model. Finally, it can be deduced that these natural materials are effective and safe adsorbents for the removal of pollutants.

Acknowledgements. The authors thank Islamic Azad University, Khorramabad Branch.

Conflicts of interest. The authors declare none.

References

- Abbou B., Lebkiri I., Ouaddari H., Kadiri L., Ouass A., Elamri A., *et al.* (2022) Study of the adsorption performance of a cationic dye onto a Moroccan clay. *Journal of Chemical Health Risks*, **4**, 563–574.
- Adebowale K.O., Olu-Owolabi B.I. & Chigbundu E.C. (2014) Removal of safranin-O from aqueous solution by adsorption onto kaolinite clay. *Journal of Encapsulation and Adsorption Sciences*, **4**, 89–104.
- Akbar S., Akhtar M.A., Khan A., Jilani G., Fashina B. & Deng Y. (2022) Aflatoxin adsorption by natural and heated sepiolite and palygorskite in comparison with adsorption by smectite. *Clays and Clay Minerals*, **70**, 733–752.
- Albroomi H.I., Elsayed M.A., Baraka A. & Abdelmaged M.A. (2016) Batch and fixed-bed adsorption of tartrazine azo-dye onto activated carbon prepared from apricot stones. *Applied Water Science*, **7**, 2063–2074.
- Alkherraz A.M., Elsherif K.M. & Blyblo N.A. (2023) Safranin adsorption onto *Acacia* plant derived activated carbon: isotherms, thermodynamics and kinetic studies. *Chemistry International*, **9**, 134–145.
- Amrhar O., Berisha A., Gana L.E., Nassali H. & Elyoubi M.S. (2023) Removal of methylene blue dye by adsorption onto natural muscovite clay: experimental, theoretical and computational investigation. *International Journal of Environmental Analytical Chemistry*, **103**, 2419–2444.
- Azad F.N., Ghaedi M., Dashtian K., Hajati S., Goudarzi A. & Jamshidi M. (2015) Enhanced simultaneous removal of malachite green and safranin O by ZnO nanorod-loaded activated carbon: modeling, optimization and adsorption isotherms. *New Journal of Chemistry*, **39**, 7998–8005.
- Azizpourian M., Kouchakzadeh G. & Derikvand Z. (2023) Removal of pharmaceutical compounds from aqueous solution by clay-based synthesized adsorbents: adsorption kinetics and isotherms studies. *Chemical Papers*, **77**, 4245–4264.
- Baccar R., Sarrà M., Bouzid J., Feki M. & Blázquez P. (2012) Removal of pharmaceutical compounds by activated carbon prepared from agricultural by-product. *Chemical Engineering Journal*, **211–212**, 310–317.
- Baloyi J., Ntho T. & Moma J. (2018) Synthesis and application of pillared clay heterogeneous catalysts for wastewater treatment: a review. *RSC Advances*, **8**, 5197–5211.
- Banerjee P., Das P., Zaman A. & Das P. (2016) Application of graphene oxide nanoplatelets for adsorption of Ibuprofen from aqueous solutions: evaluation of process kinetics and thermodynamics. *Process Safety and Environmental Protection*, **101**, 45–53.
- Bassir S.M. & Shadzadeh S.R. (2020) Static adsorption of a new cationic biosurfactant on carbonate minerals: application to EOR. *Petroleum Science and Technology*, **38**, 462–471.
- Bensalah J., Habsaoui A., Dagdag O., Lebkiri A., Ismi I., Rifi E.H. *et al.* (2021) Adsorption of a cationic dye (safranin) by artificial cationic resins Amberlite®IRC-50: equilibrium, kinetic and thermodynamic study. *Chemical Data Collections*, **35**, 100756.
- Bentahar S., Dbik A., Khomri M.E., Messaoudi N.E. & Lacherai A. (2018) Removal of a cationic dye from aqueous solution by natural clay. *Groundwater for Sustainable Development*, **6**, 255–262.
- Bergaya F. & Lagaly G. (2006) General introduction: clays, clay minerals, and clay science. Pp. 1–18 in: *Handbook of Clay Science* (F. Bergaya, B.K.G. Theng & G. Lagaly, editors). Elsevier, Amsterdam, The Netherlands.
- Bernal V., Giraldo L. & Moreno-Piraján J.C. (2020) Adsorption of pharmaceutical aromatic pollutants on heat-treated activated carbons: effect of carbonaceous structure and the adsorbent–adsorbate interactions. *ACS Omega*, **5**, 15247–15256.
- Bhatnagar A., Vilar V.J.P., Botelho C.M.S. & Boaventura R.A.R. (2010) Coconut-based biosorbents for water treatment – a review of the recent literature. *Advances in Colloid Interface Science*, **160**, 1–15.
- Boudriche L., Calvet R., Hamdi B. & Balard H. (2011) Effect of acid treatment on surface properties evolution of attapulgite clay: an application of inverse gas chromatography. *Colloids and Surfaces A: Physicochemical and Engineering Aspects*, **392**, 45–54.
- Braja M.D. & Dean E. (2012) *Principles of Geotechnical Engineering* (8th edition). Cengage Learning, Boston, MA, USA, 766 pp.
- Campos N.F., Barbosa C.M.B.M., Rodríguez-Díaz J.M. & Duarte M.M.M.B. (2018) Removal of naphthenic acids using activated charcoal: kinetic and equilibrium studies. *Adsorption Science & Technology*, **36**, 1405–1421.
- Cardona Y., Korili S. & Gil A. (2023) Use of clays and pillared clays in the catalytic photodegradation of organic compounds in aqueous solutions. *Catalysis Reviews*, **10.1080/01614940.2023.2178736**.
- Casti F., Basoccu F., Mocchi R., De Luca L., Porcheddu A. & Cuccu F. (2022) Appealing renewable materials in green chemistry. *Molecules*, **27**, 1988.
- Chakravarty R. & Banerjee P. (2012) Mechanism of cadmium binding on the cell wall of an acidophilic bacterium. *Bioresource Technology*, **108**, 176–183.
- Chen Z., Jin X., Chen Z., Megharaj M. & Naidu R. (2011) Removal of methyl orange from aqueous solution using bentonite-supported nanoscale zero-valent iron. *Journal of Colloid and Interface Science*, **363**, 601–607.
- Chisholm H. (1911) Safarine. P. 1000 in: *Encyclopaedia Britannica*, vol. **23** (11th ed.). Cambridge University Press, Cambridge, UK.
- Choi H., Choi H., Inoue M. & Sengoku R. (2017) Control of the polymorphism of calcium carbonate produced by self-healing in the cracked part of cementitious materials. *Applied Sciences*, **7**, 546.
- Chowdhury P. & Viraraghavan T. (2009) Sonochemical degradation of chlorinated organic compounds, phenolic compounds and organic dyes – a review. *Science of the Total Environment*, **407**, 2474–2492.

- Christidis G.E. (2012). Industrial clays. Pp. 341–414 in: *Advances in the Characterization of Industrial Minerals* (G.E. Christidis, editor). The Mineralogical Society of Great Britain and Northern Ireland, Twickenham, UK.
- Derikvand Z., Akbari S., Kouchakzadeh G., Azadbakht A. & Nemati A. (2019) High performance removal of azo and cationic dyes pollutants with Mn-aluminophosphate particles: kinetics, thermodynamics, and adsorption equilibrium studies. *Russian Journal of Physical Chemistry A*, **93**, 2604–2612.
- Ding M., Zuo S. & Qi C. (2015) Preparation and characterization of novel composite AlCr-pillared clays and preliminary investigation for benzene adsorption. *Applied Clay Science*, **115**, 9–16.
- Duan Y., Song Y. & Zhou L. (2019) Facile synthesis of polyamidoamine dendrimer gel with multiple amine groups as a super adsorbent for highly efficient and selective removal of anionic dyes. *Journal of Colloid and Interface Science*, **546**, 351–360.
- Edet U.A. & Ifelebuegu A.O. (2020) Kinetics, isotherms, and thermodynamic modeling of the adsorption of phosphates from model wastewater using recycled brick waste. *Processes*, **8**, 665.
- El-Kemary M., Abdel-Moneam Y.K., Madkour M. & El-Mehasseb I.M. (2011) Enhanced photocatalytic degradation of safranin-O by heterogeneous nanoparticles for environmental applications. *Journal of Luminescence*, **131**, 570–576.
- Elaiyappillai E., Meena B.C., Renuka N., Santhiya M., George J., Kanimozhi E.P. *et al.* (2021) Walnut shell derived mesoporous activated carbon for high performance electrical double layer capacitors. *Journal of Electroanalytical Chemistry*, **901**, 115762.
- Fayazi M., Afzali D., Taher M.A., Mostafavi A. & Gupta V.K. (2015) Removal of safranin dye from aqueous solution using magnetic mesoporous clay: optimization study. *Journal of Molecular Liquids*, **212**, 675–685.
- Foo K. & Hameed B. (2010) Insights into the modeling of adsorption isotherm systems. *Chemical Engineering Journal*, **156**, 2–10.
- Gillott J. (1987) Physical chemistry of clays. Pp. 143–166 in: *Clay in Engineering Geology* (J.E. Gillott, editor), Development in Geotechnical Engineering, 41. Elsevier, Amsterdam, The Netherlands.
- Guo F., Aryana S.A., Han Y. & Jiao Y. (2018) A review of the synthesis and applications of polymer-nanoclay composites. *Applied Sciences*, **8**, 1696.
- Guo F., Liu Y., Wang H., Zeng G., Hu X., Zheng B. *et al.* (2015) Adsorption behavior of Cr(VI) from aqueous solution onto magnetic graphene oxide functionalized with 1,2-diaminocyclohexanetetraacetic acid. *RSC Advances*, **5**, 45384–45392.
- Gupta V.K., Jain R., Nayak A., Agarwal S. & Shrivastava M. (2011) Removal of the hazardous dye – tartrazine by photodegradation on titanium dioxide surface. *Materials Science and Engineering: C*, **31**, 1062–1067.
- Haleta A.M.B., Catrinescu C. & Macoveanu M. (2009) Adsorption of *n*-hexane vapors onto non-functionalized hypercrosslinked polymers (Hypersol-Macronet™) and activated carbon: equilibrium studies. *Environmental Engineering and Management Journal*, **8**, 173–181.
- Haoue S., Dardar H., Belbachir M. & Harrane A. (2020) Polymerization of ethylene glycol dimethacrylate (EGDM), using an Algerian clay as cocatalyst (Maghnite-H⁺ and Maghnite-NA₂). *Bulletin of Chemical Reaction Engineering*, **15**, 221–230.
- Hebert J., Wang L., Wang X., Baker J., Rivera N., Troedel M. & Li Z. (2020) Mechanisms of safranin O interaction with 1:1 layered clay minerals. *Separation Science and Technology*, **56**, 1985–1995.
- Hongsawat P. & Prarat P. (2022) Comparative adsorption performance of oxytetracycline and sulfamethoxazole antibiotic on powder activated carbon and graphene oxide. *Chemical Papers*, **76**, 2293–2305.
- Irandoost M., Pezeshki-Modaress M. & Javanbakht V. (2019). Removal of lead from aqueous solution with nanofibrous nanocomposite of polycaprolactone adsorbent modified by nanoclay and nanozeolite. *Journal of Water Process Engineering*, **32**, 100981.
- Ismail W.N.W. & Mokhtar S.U. (2021) Various methods for removal, treatment, and detection of emerging water contaminants. Ch. 3 in: *Emerging Contaminants* (A. Nuro, editor). IntechOpen, London, UK.
- İyim T.B. & Güçlü G. (2009) Removal of basic dyes from aqueous solutions using natural clay. *Desalination*, **249**, 1377–1379.
- Kamaraj C., Lakshmi S., Rose C. & Muralidharan C. (2017) Wet blue fiber and lime from leather industry solid waste as stabilizing additive and filler in design of stone matrix asphalt. *Asian Journal of Research in Social Sciences and Humanities*, **7**, 240.
- Karthikeyan S., Sivakumar B. & Sivakumar N. (2010) Film and pore diffusion modeling for adsorption of Reactive Red 2 from aqueous solution on to activated carbon prepared from bio-diesel industrial waste. *E-Journal of Chemistry*, **7**, S175–S184.
- Kassimi A.E., Achour Y., Himri M.E., Laamari R. & Haddad M.E. (2021) Removal of two cationic dyes from aqueous solutions by adsorption onto local clay: experimental and theoretical study using DFT method. *International Journal of Environmental Analytical Chemistry*, **103**, 1223–1244.
- Kaur S., Rani S., Mahajan R.K., Asif M. & Gupta V.K. (2015) Synthesis and adsorption properties of mesoporous material for the removal of dye safranin: kinetics, equilibrium, and thermodynamics. *Journal of Industrial and Engineering Chemistry*, **22**, 19–27.
- Kilislioglu A. & Aras G. (2010) Adsorption of uranium from aqueous solution on heat and acid treated sepiolites. *Applied Radiation and Isotopes*, **68**, 2016–2019.
- Kuang Y., Zhang X. & Zhou S. (2020) Adsorption of methylene blue in water onto activated carbon by surfactant modification. *Water*, **12**, 587.
- Kyzas G.Z. & Kostoglou M. (2014) Green adsorbents for wastewaters: a critical review. *Materials*, **7**, 333–364.
- Langmuir I. (1918) The adsorption of gases on plane surfaces of glass, mica and platinum. *Journal of the American Chemical Society*, **40**, 1361–1403.
- Largitte L. & Pasquier R. (2016) A review of the kinetics adsorption models and their application to the adsorption of lead by an activated carbon. *Chemical Engineering Research and Design*, **109**, 495–504.
- Lezehari M., Basly J., Baudu M. & Bouras O. (2010) Alginate encapsulated pillared clays: removal of a neutral/anionic biocide (pentachlorophenol) and a cationic dye (safranin) from aqueous solutions. *Colloids and Surfaces A: Physicochemical and Engineering Aspects*, **366**, 88–94.
- Lima É.C., Sher F., Guleria A., Saeb M.R., Anastopoulos I., Tran H.N. & Hosseini-Bandegharai A. (2021) Is one performing the treatment data of adsorption kinetics correctly? *Journal of Environmental Chemical Engineering*, **9**, 104813.
- López-Chavez M.C., Osorio-Revilla G., Arellano-Cárdenas S., Gallardo-Velázquez T., Flores-Valle S.O. & López-Cortez MS. (2017) Preparation of starch/clay/glycerol nanocomposite films and their FTIR, XRD, SEM and mechanical characterizations. *Revista Mexicana de Ingeniería Química*, **16**, 793–804.
- Mahdi A.B., Aljeboree A.M. & Alkaim A.F. (2021) Adsorption and removal of pollutants (dyes) from wastewater using different types of low-cost adsorbents: a review. *Journal of Chemical Health Risks*, **11**, 203–212.
- Mahmoud M.E., Abdelfattah A.M., Tharwat R.M. & Nabil G.M. (2020) Adsorption of negatively charged food tartrazine and sunset yellow dyes onto positively charged triethylenetetramine biochar: optimization, kinetics and thermodynamic study. *Journal of Molecular Liquids*, **318**, 114297.
- Manjuladevi M., Anitha R. & Manonmani S. (2018) Kinetic study on adsorption of Cr(VI), Ni(II), Cd(II) and Pb(II) ions from aqueous solutions using activated carbon prepared from *Cucumis melo* peel. *Applied Water Science*, **8**, 36.
- Marsh A., Heath A., Patureau P., Evernden M. & Walker P. (2019) Phase formation behaviour in alkali activation of clay mixtures. *Applied Clay Science*, **175**, 10–21.
- Mohamed F. & Abukhadra M.R. (2018) Removal of safranin dye from water using polypyrrole nanofiber/Zn-Fe layered double hydroxide nanocomposite (Ppy NF/Zn-Fe LDH) of enhanced adsorption and photocatalytic properties. *Science of the Total Environment*, **640–641**, 352–363.
- Mohan C., Kumari P., Kumari N. & Negi A. (2023) Fabrication of colored polymeric membrane using clay-based nano pigments of safranin O (SO) dye. *Membranes*, **13**, 619.
- Mondal S., Aikat K. & Halder G. (2016) Biosorptive uptake of Ibuprofen by chemically modified *Parthenium hysterophorus* derived biochar: equilibrium, kinetics, thermodynamics and modeling. *Ecological Engineering*, **92**, 158–172.
- Moradi M., Moradkhani M., Hosseini S.H. & Olazar M. (2022). Intelligent modeling of photocatalytically Reactive Yellow 84 azo dye removal from aqueous

- solutions by ZnO-light expanded clay aggregate nanoparticles. *International Journal of Environmental Science and Technology*, **20**, 3009–3022.
- Morrison A.B., Strezov V., Niven R.K., Taylor M.P., Wilson S.P., Wang J. *et al.* (2023) Impact of salinity and temperature on removal of PFAS species from water by aeration in the absence of additional surfactants: a novel application of green chemistry using adsorptive bubble fractionation. *Industrial & Engineering Chemistry Research*, **62**, 5635–5645.
- Natal J.P.S., Cusioli L.F., Magalhães-Ghiotto G.A.V., Bergamasco R. & Gomes R.G. (2023) Removal of methylene blue and safranin orange pollutants from liquid effluents by soy residue. *Canadian Journal of Chemical Engineering*, **101**, 5561–5575.
- Njaramba L.K., Kim M., Yea Y., Yoon Y. & Park C.M. (2023) Efficient adsorption of naproxen and ibuprofen by gelatin/zirconium-based metal-organic framework/sepilolite aerogels via synergistic mechanisms. *Chemical Engineering Journal*, **452**, 139426.
- Nooryazdan A. & Ghobadi M.H. (2019) The Landslide Lake of Jaydar. *Journal of Earth Science & Climate Change*, **10**, 507.
- Nourmoradi H., Moghadam K.F., Jafari A. & Kamarehie B. (2018) Removal of acetaminophen and ibuprofen from aqueous solutions by activated carbon derived from *Quercus brantii* (oak) acorn as a low-cost biosorbent. *Journal of Environmental Chemical Engineering*, **6**, 6807–6815.
- Obradović B. (2020) Guidelines for general adsorption kinetics modeling. *Hemjska Industrija*, **74**, 65–70.
- Panda A.K., Mishra B.G., Mishra D.K. & Singh R. (2010) Effect of sulphuric acid treatment on the physico-chemical characteristics of kaolin clay. *Colloids and Surfaces A: Physicochemical and Engineering Aspects*, **363**, 98–104.
- Pap S., Kirk C.A., Bremner B., Sekulić M.T., Shearer L., Gibb S.W. & Taggart M.A. (2020) Low-cost chitosan-calcite adsorbent development for potential phosphate removal and recovery from wastewater effluent. *Water Research*, **173**, 115573.
- Perri F., Cirrincione R., Critelli S., Mazzoleni P. & Pappalardo A. (2008) Clay mineral assemblages and sandstone compositions of the Mesozoic Longobucco Group, northeastern Calabria: implications for burial history and diagenetic evolution. *International Geology Review*, **50**, 1116–1131.
- Pouretedal H.R. & Sadeh N. (2014) Effective removal of amoxicillin, cephalexin, tetracycline and penicillin G from aqueous solutions using activated carbon nanoparticles prepared from vine wood. *Journal of Water Process Engineering*, **1**, 64–73.
- Rezende J.C.T., Ramos V.H.S., De Oliveira H.A., Oliveira R.M.P.B. & De Jesús E. (2018) Removal of Cr(VI) from aqueous solutions using clay from Calumbi Geological Formation, N. Sra. Socorro, SE State, Brazil. *Materials Science Forum*, **912**, 1–6.
- Roosta M., Ghaedi M. & Yousefi F. (2015) Optimization of the combined ultrasonic assisted/adsorption method for the removal of malachite green by zinc sulfide nanoparticles loaded on activated carbon: experimental design. *RSC Advances*, **5**, 100129–100141.
- Ruiz-Agudo E., Álvarez-Lloret P., Ibáñez-Velasco A. & Ortega-Huertas M. (2016) Crystallographic control in the replacement of calcite by calcium sulfates. *Crystal Growth & Design*, **16**, 4950–4959.
- Saha N., Das L., Das P., Bhowal A. & Bhattacharjee C. (2021) Comparative experimental and mathematical analysis on removal of dye using raw rice husk, rice husk charcoal and activated rice husk charcoal: batch, fixed-bed column, and mathematical modeling. *Biomass Conversion and Biorefinery*, **13**, 11023–11040.
- Sayed M.Y.E., Abdel-Gaber A.M. & Rahal H.T. (2019) Safranin – a potential corrosion inhibitor for mild steel in acidic media: a combined experimental and theoretical approach. *Journal of Failure Analysis and Prevention*, **19**, 1174–1180.
- Sepehr M.N., Amrane A., Karimaian K.A., Zarrabi M. & Ghaffari H.R. (2014) Potential of waste pumice and surface modified pumice for hexavalent chromium removal: characterization, equilibrium, thermodynamic and kinetic study. *Journal of the Taiwan Institute of Chemical Engineers*, **45**, 635–647.
- Shaltout W.A., El-Naggar G.A., Esmail G. & Hassan A.F. (2024) Synthesis and characterization of ferric@nanocellulose/nanohydroxyapatite bio-composite based on sea scallop shells and cotton stalks: adsorption of safranin-O dye. *Biomass Conversion and Biorefinery*, **14**, 4759–4776.
- Sharma M., Mishra N., Bansal S., Siddiqui A.M. & Khanuja M. (2024) Efficient adsorption and photocatalytic degradation of textile dye from metal ion-substituted ferrite for environmental remediation. *International Journal of Environmental Science and Technology*, **21**, 6075–6092.
- Sharma P., Kaur H., Sharma M. & Sahore V. (2011) A review on applicability of naturally available adsorbents for the removal of hazardous dyes from aqueous waste. *Environmental Monitoring and Assessment*, **183**, 151–195.
- Shi Y., Wang X., Wang X., Carlson K. & Li Z. (2021) Removal of toluidine blue and safranin O from single and binary solutions using zeolite. *Crystals*, **11**, 1181.
- Shirsath S.R., Hage A., Zhou M., Sonawane S.H. & Ashokkumar M. (2011) Ultrasound assisted preparation of nanoclay bentonite-FeCo nanocomposite hybrid hydrogel: a potential responsive sorbent for removal of organic pollutant from water. *Desalination*, **281**, 429–437.
- Shivaraju H.P., Egumbo H., Madhusudan P., Kumar K. & Midhun G. (2018) Preparation of affordable and multifunctional clay-based ceramic filter matrix for treatment of drinking water. *Environmental Technology*, **40**, 1633–1643.
- Shrivastava R., Jain S.R. & Frank S.G. (1985) Dissolution dialysis studies of metronidazole-montmorillonite adsorbates. *Journal of Pharmaceutical Sciences*, **74**, 214–216.
- Shwan D.M.S. (2022) Characterization of local natural clay and its using for adsorption removal of gram stain wastes (safranin-O and Crystal Violet) from microbiological laboratories. *Iranian Journal of Science*, **47**, 63–71.
- Sieren B., Baker J., Wang X., Rozzoni S.J., Carlson K., McBain A. *et al.* (2020) Sorptive removal of color dye safranin O by fibrous clay minerals and zeolites. *Advances in Materials Science and Engineering*, **2020**, 1–12.
- Silva D.L., Balaba N., Horsth D.F.L., Jaeger S. & Anaissi F.J. (2023) Characterization of calcined red soil applied in the removal of methylene blue dye from wastewater to produce a hybrid pigment. *Clay Minerals*, **58**, 83–94.
- Suleman M., Zafar M., Ahmed A., Rashid M.U., Hussain S., Razzaq A. *et al.* (2021). Castor leaves-based biochar for adsorption of safranin from textile wastewater. *Sustainability*, **13**, 6926.
- Tezcanli-Güyer G. & Ince N.H. (2004) Individual and combined effects of ultrasound, ozone and UV irradiation: a case study with textile dyes. *Ultrasonics*, **42**, 603–609.
- Uğraşkan V., Işık B., Yazıcı Ö. & Çakar F. (2022) Removal of safranin T by a highly efficient adsorbent (*Cotinus coggygia* leaves): isotherms, kinetics, thermodynamics, and surface properties. *Surfaces and Interfaces*, **28**, 101615.
- Uygun O., Murat A. & Çakal G.Ö. (2023) Magnetic sepilolite/iron(III) oxide composite for the adsorption of lead(II) ions from aqueous solutions. *Clay Minerals*, **58**, 267–279.
- Vicente M., Gil A. & Bergaya F. (2013) Pillared clays and clay minerals. Pp. 523–557 in: *Handbook of Clay Science* (F. Bergaya, B.K.G. Theng & G. Lagaly, editors). Elsevier, Amsterdam, The Netherlands.
- Viftaria M., Nurhayati N. & Anita S. (2019) Surface acidity of sulfuric acid activated Maredan clay catalysts with Boehm titration method and pyridine adsorption-FTIR. *Journal of Physics: Conference Series*, **1351**, 012040.
- Wahab N., Saeed M., Ibrahim M., Munir A., Saleem M., Zahra M. & Waseem A. (2019) Synthesis, characterization, and applications of silk/bentonite clay composite for heavy metal removal from aqueous solution. *Frontiers in Chemistry*, **7**, 654.
- Wang Z., Zhao Q., Wang D. & Cui C. (2021) Synthesis and characterization of ordered mesoporous MCM-41 from natural chlorite and its application in methylene blue adsorption. *Clays and Clay Minerals*, **69**, 217–231.
- Xu J., Wang L. & Zhu Y. (2012) Decontamination of bisphenol A from aqueous solution by graphene adsorption. *Langmuir*, **28**, 8418–8425.
- Yarmohammadi N., Ghadermazi M., Derikvand Z. & Mozafari R. (2022) *In situ* synthesis of bimetallic γ -Fe₂O₃/Cu nanoparticles over pectin hydrogel obtained from biomass resource (orange peel) as a reusable green catalyst for oxidation and C–S cross-coupling reactions. *Chemical Papers*, **76**, 4289–4307.

- Yin J., Deng C., Yu Z., Wang X. & Xu G. (2018) Effective removal of lead ions from aqueous solution using nano illite/smectite clay: isotherm, kinetic, and thermodynamic modeling of adsorption. *Water*, **10**, 210.
- Yurtay A. & Kılıç M. (2023) Biomass-based activated carbon by flash heating as a novel preparation route and its application in high efficiency adsorption of metronidazole. *Diamond and Related Materials*, **131**, 109603.
- Zawrah M., Khattab R., Saad E. & Gado R. (2014) Effect of surfactant types and their concentration on the structural characteristics of nanoclay. *Spectrochimica Acta Part A: Molecular and Biomolecular Spectroscopy*, **122**, 616–623.
- Zeng P., Nie X., Qin Z., Luo S., Fu Y., Yu W. *et al.* (2023) Adsorption of gold nanoparticles on illite under high solid/liquid ratio and initial pH conditions. *Clay Minerals*, **58**, 245–257.
- Żółtowska-Aksamitowska S., Bartczak P., Zembrzuska J. & Jesionowski T. (2018) Removal of hazardous non-steroidal anti-inflammatory drugs from aqueous solutions by biosorbent based on chitin and lignin. *Science of the Total Environment*, **612**, 1223–1233.